Spectral properties of a Ξ-configuration atom driven by a pair of bichromatic fields*

Jin Kang(金 康)[a)b)c)†], Xie Xiao-Tao(谢小涛)[a)b)c)], and Jiang Zhen-Yi(姜振益)[d)]

[a)] *Department of Physics, Northwest University, Xi'an* 710069, *China*
[b)] *National photoelectric technology and Functional Materials & Application of Science and Technology International Cooperation Base, Xi'an* 710069, *China*
[c)] *National Key Laboratory of Photoelectric Technology and Functional Materials (Culture Base), Xi'an* 710069, *China*
[d)] *Institute of Modern Physics, Northwest University, Xi'an* 710069, *China*

(Received 31 March 2012; revised manuscript received 27 July 2012)

The absorption spectrum and the incoherent fluorescence spectrum of the lower transition in an Ξ-configuration three-level atomic system driven by a pair of bichromatic fields is investigated. The transmission of the absorption profile from a multipeaked feature to a single-peak feature is identified. Adjusting the relative phase between the two driving fields, the splitting effects of the spectral peaks occur both in the fluorescence and the absorption spectra. Furthermore, phase modulating can dramatically lead to a great suppression of the amplitudes of the whole absorption spectrum. Physically, this effect is attributed to the phase-sensitive nature of the populations and coherence between the atomic states of the system.

Keywords: bichromatic field, phase modulating, degradation of absorption, splitting effect

PACS: 42.50.Gy, 42.50.–p **DOI:** 10.1088/1674-1056/22/1/014205

1. Introduction

The interaction of a polychromatic field with an atomic system is an important subject in quantum optics and nonlinear optics. In early studies, researchers found that when more than one driving fields are introduced to a two-level atomic system, the atomic system will demonstrate many novel optical effects, including a multipeaked absorption and fluorescence spectrum,[1–4] the transmission of the fluorescence spectrum from a multipeaked structure to a Mollow triplet,[5] noise squeezing,[6] and probe-intensity-related absorptive, dispersive behaviors,[7] etc. It has been proved that these new effects are directly related to the dressed-state structure of the system. Some recent studies about the optical properties of three-level atoms driven by a bichromatic field revealed various new effects. The experimental research in a Λ atomic system using a bichromatic driving field demonstrated the EIT phenomenon with an improved controllability.[8] Also in the Λ system, with an appropriate choice for the detuning of the bichromatic field, the absorption spectrum shows a feature consisting of symmetric doublets.[9] Some other configurations of atomic systems driven by polychromatic fields are also discussed.[10–12] More recently, some researchers' works show that some new effects in the medium driven by a bichromatic field have promising importance in some optical information processes such as quantum memory,[13] bright entangled source of light,[14] bichromatic pulse propagating,[15] and some other related technologies including high-precision EIT vector magnetometer,[16] atom interferometer,[17] and attosecond pulse generation.[18]

As we know, when polychromatic field driving is introduced, the system always demonstrates a variety of phase-dependent behavior, such as phase-dependent absorptive profile,[19,20] coherent population trapping,[21] manipulation of Kerr nonlinearity,[22] and coherent phase control in electron scattering.[23] Some researches showed that phase-dependent behavior also can be caused by a single laser pulse in the strong-field regime, in which the carrier-envelope phase (CEP) of the laser pulse plays a crucially important role.[24–26] In a word, the study on the phase dependent effects in optical physics is still a valuable issue and further research will help us deepen the understanding of coherent control.

In this paper, we study the absorption spectrum and the incoherent fluorescence spectra of the lower transition of an Ξ-configuration system in which the whole system is driven by a pair of bichromatic fields. It should be noted that in Ref. [12], the authors showed several interesting effects in the incoherent fluorescence spectrum in an Ξ-configuration system driven by a pair of bichromatic fields, e.g., the elimination of the fluorescence decay and the selective elimination of the spectral lines. In contrast to their investigations, our study on the fluorescence spectrum of the system focuses on the influences of the second bichromatic field applied to one dipole transition on the fluorescence spectrum of another dipole transition, so that

*Project supported by the National Natural Science Foundation of China (Grant Nos. 61008016, 10647008, and 50971099), the Natural Science Basis Research Plan in Shaanxi Province of China (Grant No. 2010JQ1002), the Education Department of Shaanxi Province, China (Grant Nos. 09JK752 and 11JK0550), and the Doctoral Program Foundation of Institutions of Higher Education of China (Grant No. 20106101120020).

†Corresponding author. E-mail: jinkang@nwu.edu.cn

© 2013 Chinese Physical Society and IOP Publishing Ltd

the modulation of the intensity of one bichromatic field, which will lead to the variations of the eigenstates of the system, are taken into account. We present the steady-state spectra graphically and the corresponding explanations. The article is organized as follows: in Section 2, the model is described and the numerical results of the absorption and fluorescence spectrum are presented; in Section 3, the spectra are investigated in detail through a dressed-atom description; in Section 4, a brief summary is given.

2. Theoretical model, density-matrix equations, and absorption spectra

The system under investigation is a three-level Ξ-configuration atom which is driven by a pair of bichromatic fields, as shown in Fig. 1. The top, intermediate, and bottom states are denoted by $|1\rangle$, $|2\rangle$, and $|3\rangle$, respectively. A bichromatic field $\boldsymbol{E}_a = \boldsymbol{E}_1 \mathrm{e}^{-\mathrm{i}\omega_1 t+\mathrm{i}\phi_1} + \boldsymbol{E}_3 \mathrm{e}^{-\mathrm{i}\omega_3 t+\mathrm{i}\phi_3}$ is applied to render the transition $|1\rangle \leftrightarrow |2\rangle$ with energy gap $\hbar\omega_{12}$, and another bichromatic field $\boldsymbol{E}_b = \boldsymbol{E}_2 \mathrm{e}^{-\mathrm{i}\omega_2 t+\mathrm{i}\phi_2} + \boldsymbol{E}_4 \mathrm{e}^{-\mathrm{i}\omega_4 t+\mathrm{i}\phi_4}$ is used to induce the transition $|2\rangle \leftrightarrow |3\rangle$ with energy gap $\hbar\omega_{23}$. Therein ϕ_1, ϕ_2, ϕ_3, and ϕ_4 are the initial phases of the four driving fields, respectively. We assume the frequencies of the two fields satisfy the two-photon resonance, i.e., $\omega_1+\omega_2 = \omega_3+\omega_4 = \omega_{12}+\omega_{23}$. In this condition, the driven fields can be expressed as

$$\begin{aligned}\boldsymbol{E}_a &= (\boldsymbol{E}_1 \mathrm{e}^{-\mathrm{i}\delta t+\mathrm{i}\phi_1} + \boldsymbol{E}_3 \mathrm{e}^{\mathrm{i}\delta t+\mathrm{i}\phi_3})\mathrm{e}^{-\mathrm{i}\omega_{12}t},\\ \boldsymbol{E}_b &= (\boldsymbol{E}_2 \mathrm{e}^{\mathrm{i}\delta t+\mathrm{i}\phi_3} + \boldsymbol{E}_4 \mathrm{e}^{-\mathrm{i}\delta t+\mathrm{i}\phi_4})\mathrm{e}^{-\mathrm{i}\omega_{23}t},\end{aligned}$$

where δ is the detuning. Here we assume that symmetrically detuned fields were applied, i.e., $\omega_1-\delta = \omega_3+\delta = \omega_{12}$. The strength of the coupling is given by the Rabi frequency $\Omega_i \mathrm{e}^{\mathrm{i}\phi_i}$ ($i = 1,2,3,4$), where Ω_i is real. The evolutions of the atomic states at time t are described by the density matrix ρ, which obeys the following master equation:

$$\frac{\mathrm{d}}{\mathrm{d}t}\rho = \frac{1}{\mathrm{i}\hbar}[H,\rho] + \mathscr{L}\rho. \tag{1}$$

Here, the Hamiltonian H reads

$$\begin{aligned}H &= \hbar[\omega_{23}\sigma_{22} + (\omega_{23}+\omega_{12})\sigma_{11}]\\ &\quad -\hbar[(\Omega_1 \mathrm{e}^{-\mathrm{i}\delta t+\mathrm{i}\phi_1} + \Omega_3 \mathrm{e}^{\mathrm{i}\delta t+\mathrm{i}\phi_3})\mathrm{e}^{-\mathrm{i}\omega_{12}t}\sigma_{12}\\ &\quad +(\Omega_2 \mathrm{e}^{\mathrm{i}\delta t+\mathrm{i}\phi_2} + \Omega_4 \mathrm{e}^{-\mathrm{i}\delta t+\mathrm{i}\phi_4})\mathrm{e}^{-\mathrm{i}\omega_{23}t}\sigma_{23} + \mathrm{c.c.}],\end{aligned} \tag{2}$$

where $\sigma_{mn} \equiv |m\rangle\langle n|$ ($m,n = 1,2,3$) is the transition operator. The relaxation processes are assumed to be radiative and described by the Liouvillian $\mathscr{L}\rho$ which has the form

$$\begin{aligned}\mathscr{L}\rho &= -\gamma_1\sigma_{12}\sigma_{21}\rho - \gamma_2\sigma_{23}\sigma_{32}\rho -\\ &\quad +2\gamma_1\sigma_{21}\rho\ \sigma_{12} + 2\gamma_2\sigma_{23}\rho\sigma_{32}\\ &\quad -\gamma_1\rho\sigma_{12}\sigma_{21} - \gamma_2\rho\sigma_{23}\sigma_{32},\end{aligned} \tag{3}$$

where γ_1 and γ_2 are decay rates from $|1\rangle$ to $|2\rangle$, and from $|2\rangle$ to $|3\rangle$, respectively.

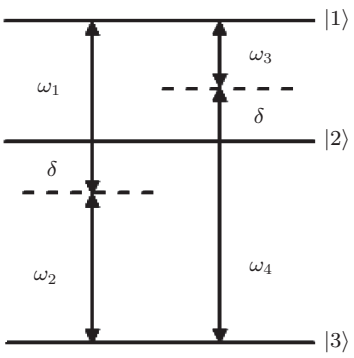


Fig. 1. Schematic diagram of a three-level Ξ-type system driven by a pair of bichromatic fields.

The Hamiltonian (2) is explicitly relevant to the phases of the driving fields because there is no reference frame in which the phases dependence can be eliminated. By introducing the frame rotating $|2\rangle \to \mathrm{e}^{-\mathrm{i}\omega_{23}t+i\phi_1}|2\rangle$ and $|1\rangle \to \mathrm{e}^{-\mathrm{i}(\omega_{23}+\omega_{12})t+\mathrm{i}\phi_2+\mathrm{i}\phi_1}|1\rangle$, we can rewrite the Hamiltonian (2) as

$$\begin{aligned}\widetilde{H} &= -\hbar[(\Omega_1 \mathrm{e}^{-\mathrm{i}\delta t} + \Omega_3 \mathrm{e}^{\mathrm{i}\delta t-\mathrm{i}\phi_\mathrm{A}})\sigma_{12}\\ &\quad +(\Omega_2 \mathrm{e}^{\mathrm{i}\delta t} + \Omega_4 \mathrm{e}^{-\mathrm{i}\delta t-\mathrm{i}\phi_\mathrm{B}})\sigma_{23} + \mathrm{c.c.}],\end{aligned} \tag{4}$$

where the relative phases $\phi_\mathrm{A} = \phi_1 - \phi_3$ and $\phi_\mathrm{B} = \phi_2 - \phi_4$ are defined.

For the simplicity of denomination, we still denote the density matrix with ρ in the new reference frame. The evolution is governed by the master equation

$$\frac{\mathrm{d}}{\mathrm{d}t}\rho = \frac{1}{\mathrm{i}\hbar}[\widetilde{H},\rho] + \mathscr{L}\rho. \tag{5}$$

Then the equations of motion of the corresponding density matrix elements are obtained as

$$\begin{aligned}\dot{\rho}_{11} &= -2\gamma_1\rho_{11} - b\rho_{12} - b^*\rho_{21},\\ \dot{\rho}_{22} &= 2\gamma_{11}\rho_{11} - 2\gamma_2\rho_{22} + b\rho_{12} + b^*\rho_{21} + a^*\rho_{23} + a\rho_{32},\\ \dot{\rho}_{12} &= b^*\rho_{11} + b\rho_{22} - (\gamma_1+\gamma_2)\rho_{12} + a^*\rho_{13},\\ \dot{\rho}_{13} &= -a\rho_{12} - \gamma_1\rho_{13} - b^*\rho_{23},\\ \dot{\rho}_{23} &= -a\rho_{11} - 2a\rho_{22} + b\rho_{13} - \gamma_2\rho_{23} + a,\end{aligned} \tag{6}$$

where

$$\begin{aligned}a &= \mathrm{i}\Omega_2 \mathrm{e}^{\mathrm{i}\delta t} + \mathrm{i}\Omega_4 \mathrm{e}^{-\mathrm{i}\delta t-\mathrm{i}\phi_\mathrm{B}},\\ b &= \mathrm{i}\Omega_1 \mathrm{e}^{\mathrm{i}\delta t} + \mathrm{i}\Omega_3 \mathrm{e}^{-\mathrm{i}\delta t-\mathrm{i}\phi_\mathrm{A}}.\end{aligned}$$

The density-matrix elements obey the conditions $\rho_{11}+\rho_{22}+\rho_{33} = 1$ and $\rho_{ij} = \rho_{ji}^*$, with $i,j = 1,2,3$.

The absorption spectrum of the transition $|2\rangle \leftrightarrow |3\rangle$ is calculated by

$$A(\Delta_\mathrm{p}) = \mathrm{Re}\int_0^\infty D(\tau)\mathrm{e}^{\mathrm{i}\Delta_\mathrm{p}\tau}\mathrm{d}\tau, \tag{7}$$

where

$$D(\tau)=\lim_{t\to\infty}\langle[\sigma_{32}(t+\tau),\sigma_{23}(t)]\rangle, \tag{8}$$

and $\Delta_{\rm p}$ is the detuning between the probe frequency and the atomic transition frequency ω_{23}.

In order to gain the numerical results of Eq. (7), a vector composed of a series of the average values of the two-time commutator is defined as

$$\boldsymbol{X}(\tau)=(x_1(\tau),\ldots,x_i(\tau),\ldots x_8(\tau))^{\rm T}, \tag{9}$$

where

$$x_i(\tau)=\lim_{t\to\infty}\langle[\sigma^{\rm i}(t+\tau),\sigma_{23}(t)]\rangle,\quad (i=1,2,\ldots,8), \tag{10}$$

where $\sigma^{\rm i}$ is the i-th element of vector $\boldsymbol{\sigma}$, which reads

$$\boldsymbol{\sigma}=(\sigma_{11},\sigma_{22},\sigma_{21},\sigma_{12},\sigma_{31},\sigma_{13},\sigma_{32},\sigma_{23})^{\rm T}. \tag{11}$$

According to the quantum-regression theorem, the time evolution equation of $x_i(\tau)$ has the same form as $\sigma_i(\tau)$, so that the time evolution equations of the elements of $\boldsymbol{X}(\tau)$ can be obtained from Eqs. (6). Noting that the coefficients a and b in Eqs. (6) are both time-dependent, we can decompose $x_i(\tau)$ into the form $x_i(\tau)=\sum_{l=-\infty}^{\infty}x_i^l\,{\rm e}^{{\rm i}l\delta t}$, where x_i^l represents the slowly varying amplitudes,[10] then substitute the decompositions into the equations of motion for $x_i(\tau)$, finally equate the coefficients of harmonics of δ and obtain the equations of motion of the slowly varying amplitudes x_i^l, which reads

$$\begin{aligned}
\frac{\rm d}{{\rm d}t}x_1^l &= -2\gamma_1x_1^l-il\delta x_1^l-i\Omega_1x_3^{l-1}\\
&\quad -i\Omega_3^*x_3^{l+1}+{\rm i}\Omega_3x_4^{l-1}+{\rm i}\Omega_1x_4^{l+1},\\
\frac{\rm d}{{\rm d}t}x_2^l &= 2\gamma_1x_1^l-2\gamma_2x_2^l-il\delta x_2^l+{\rm i}\Omega_1x_3^{l-1}+{\rm i}\Omega_3^*x_3^{l+1}\\
&\quad -i\Omega_3x_4^{l-1}-{\rm i}\Omega_1x_4^{l+1}-i\Omega_4^*x_7^{l-1}-i\Omega_2x_7^{l+1}\\
&\quad +{\rm i}\Omega_2x_8^{l-1}+{\rm i}\Omega_4x_8^{l+1},\\
\frac{\rm d}{{\rm d}t}x_3^l &= -{\rm i}\Omega_3x_1^{-1+l}-{\rm i}\Omega_1x_1^{1+l}+{\rm i}\Omega_3x_2^{-1+l}+{\rm i}\Omega_1x_2^{1+l}\\
&\quad -\gamma_1x_3^l-\gamma_2x_3^l-il\delta x_3^l-{\rm i}\Omega_4^*x_5^{-1+l}-{\rm i}\Omega_2x_5^{1+l},\\
\frac{\rm d}{{\rm d}t}x_4^l &= {\rm i}\Omega_1x_1^{-1+l}+{\rm i}\Omega_3^*x_1^{1+l}-{\rm i}\Omega_1x_2^{-1+l}-{\rm i}\Omega_3^*x_2^{1+l}\\
&\quad -\gamma_1x_4^l-\gamma_2x_4^l-i\delta x_4^l+{\rm i}\Omega_2x_6^{l-1}+{\rm i}\Omega_4x_6^{1+l},\\
\frac{\rm d}{{\rm d}t}x_5^l &= -{\rm i}\Omega_2x_3^{-1+l}-{\rm i}\Omega_4x_3^{1+l}-\gamma_1x_5^l-il\delta x_5^l\\
&\quad +{\rm i}\Omega_3x_7^{-1+l}+{\rm i}\Omega_1x_7^{1+l},\\
\frac{\rm d}{{\rm d}t}x_6^l &= {\rm i}\Omega_4^*x_4^{-1+l}+{\rm i}\Omega_2x_4^{1+l}-\gamma_1x_6^l-il\delta x_6^l\\
&\quad -{\rm i}\Omega_1x_8^{-1+l}-{\rm i}\Omega_3^*x_8^{1+l},\\
\frac{\rm d}{{\rm d}t}x_7^l &= {\rm i}\Omega_4\delta_{-1,l}+{\rm i}\Omega_2\delta_{1,l}-{\rm i}\Omega_2x_1^{-1+l}-{\rm i}\Omega_4x_1^{1+l}\\
&\quad -2{\rm i}\Omega_2x_2^{-1+l}-2{\rm i}\Omega_4x_2^{1+l}+{\rm i}\Omega_1x_5^{-1+l}\\
&\quad +{\rm i}\Omega_3^*x_5^{1+l}-\gamma_2x_7^l-il\delta x_7^l,\\
\frac{\rm d}{{\rm d}t}x_8^l &= -{\rm i}\Omega_2\delta_{-1,l}-{\rm i}\Omega_4^*\delta_{1,l}+{\rm i}\Omega_4x_1^{-1+l}+{\rm i}\Omega_2x_1^{1+l}\\
&\quad +2{\rm i}\Omega_4x_2^{-1+l}+2{\rm i}\Omega_2x_2^{1+l}-{\rm i}\Omega_3x_6^{-1+l}\\
&\quad -{\rm i}\Omega_1x_6^{1+l}-\gamma_2x_8^l-il\delta x_8^l.
\end{aligned} \tag{12}$$

For simplicity of expression, we label $\Omega_3\,{\rm e}^{{\rm i}\phi_{\rm A}}$ with Ω_3, and $\Omega_4\,{\rm e}^{-{\rm i}\phi_{\rm B}}$ with Ω_4, respectively. The steady values of elements in Eqs. (12) can be given by employing Laplace transform methods, which leads to the following algebraic equations for the transforms $x_i^l(z)$:

$$\begin{aligned}
(2\gamma_1+{\rm i}l\delta)x_1^l(z) &= x_1^l(0)-i\Omega_1x_3^{l-1}(z)-i\Omega_3^*x_3^{l+1}(z)\\
&\quad +{\rm i}\Omega_3x_4^{l-1}(z)+{\rm i}\Omega_1x_4^{l+1}(z),\\
(2\gamma_2+{\rm i}l\delta)x_2^l(z) &= x_2^l(0)+2\gamma_1x_1^l(z)+{\rm i}\Omega_1x_3^{l-1}(z)\\
&\quad +{\rm i}\Omega_3^*x_3^{l+1}(z)-i\Omega_3x_4^{l-1}(z)\\
&\quad -{\rm i}\Omega_1x_4^{l+1}(z)-i\Omega_4^*x_7^{l-1}(z)\\
&\quad -i\Omega_2x_7^{l+1}(z)+{\rm i}\Omega_2x_8^{l-1}(z)\\
&\quad +{\rm i}\Omega_4x_8^{l+1}(z),\\
(\gamma_1+\gamma_2+{\rm i}l\delta)x_3^l(z) &= x_3^l(0)-{\rm i}\Omega_3x_1^{-1+l}(z)-{\rm i}\Omega_1x_1^{1+l}(z)\\
&\quad +{\rm i}\Omega_3x_2^{-1+l}(z)+{\rm i}\Omega_1x_2^{1+l}(z)\\
&\quad -{\rm i}\Omega_4^*x_5^{-1+l}(z)-{\rm i}\Omega_2x_5^{1+l}(z),\\
(\gamma_1+\gamma_2+{\rm i}l\delta)x_4^l(z) &= x_4^l(0)+{\rm i}\Omega_1x_1^{-1+l}(z)+{\rm i}\Omega_3^*x_1^{1+l}(z)\\
&\quad -{\rm i}\Omega_1x_2^{-1+l}(z)-{\rm i}\Omega_3^*x_2^{1+l}(z)\\
&\quad {\rm i}\Omega_2x_6^{l-1}(z)+{\rm i}\Omega_4x_6^{1+l}(z),\\
(\gamma_1+{\rm i}l\delta)x_5^l(z) &= x_5^l(0)-{\rm i}\Omega_2x_3^{-1+l}(z)-{\rm i}\Omega_4x_3^{1+l}(z)\\
&\quad +{\rm i}\Omega_3x_7^{-1+l}(z)+{\rm i}\Omega_1x_7^{1+l}(z),\\
(\gamma_1+{\rm i}l\delta)x_6^l(z) &= x_6^l(0)+{\rm i}\Omega_4^*x_4^{-1+l}(z)+{\rm i}\Omega_2x_4^{1+l}(z)\\
&\quad -{\rm i}\Omega_1x_8^{-1+l}(z)-{\rm i}\Omega_3^*x_8^{1+l}(z),\\
(\gamma_2+{\rm i}l\delta)x_7^l(z) &= x_7^l(0)-{\rm i}\Omega_2x_1^{-1+l}(z)-{\rm i}\Omega_4^*x_1^{1+l}(z)\\
&\quad -2{\rm i}\Omega_2x_2^{-1+l}(z)-2{\rm i}\Omega_4^*x_2^{1+l}(z)\\
&\quad +{\rm i}\Omega_1x_5^{-1+l}(z)+{\rm i}\Omega_3x_5^{1+l}(z),\\
(\gamma_2+{\rm i}l\delta)x_8^l(z) &= x_8^l(0)+{\rm i}\Omega_4x_1^{-1+l}(z)+{\rm i}\Omega_2x_1^{1+l}(z)\\
&\quad +2{\rm i}\Omega_4x_2^{-1+l}(z)+2{\rm i}\Omega_2x_2^{1+l}(z)\\
&\quad -{\rm i}\Omega_3x_6^{-1+l}(z)-{\rm i}\Omega_1x_6^{1+l}(z),
\end{aligned} \tag{13}$$

where $x_i^l(0)$ are given by straightforward manipulations

$$\begin{pmatrix}x_1^l(0)\\x_2^l(0)\\x_3^l(0)\\x_4^l(0)\\x_5^l(0)\\x_6^l(0)\\x_7^l(0)\\x_8^l(0)\end{pmatrix}=\begin{pmatrix}0\\\sigma_{23}(\infty)\\0\\\sigma_{13}(\infty)\\-\sigma_{21}(\infty)\\0\\\delta_{l,0}-\sigma_{11}(\infty)-2\sigma_{22}\\0\end{pmatrix}. \tag{14}$$

Since all the steady state values in Eq. (14) can be given by numerically solving Eq. (6) by the harmonic expansion method, equation (13) can be solved without ambiguity. The absorption spectrum is given by

$$A(\Delta_{\rm p}) = {\rm Re}[x_7^0(z)|_{z={\rm i}\Delta_{\rm p}}]. \tag{15}$$

Next, we calculate the incoherent fluorescence spectrum of transition $|2\rangle \to |3\rangle$, which can be given by

$$S_{\rm in}(\Delta_{\rm f}) = {\rm Re}\int_0^\infty F(\tau){\rm e}^{{\rm i}\Delta_{\rm f}\tau}{\rm d}\tau, \tag{16}$$

where

$$F(\tau) = \lim_{t\to\infty}[\langle\sigma_{23}(t+\tau)\sigma_{32}(t)\rangle - \langle\sigma_{23}(t+\tau)\rangle\langle\sigma_{32}(t)\rangle]. \tag{17}$$

We can apply the same method mentioned above to obtain the numerical results. According to Eq. (17), we define a vector $\boldsymbol{Y}$, which is

$$\boldsymbol{Y}(\tau) = (y_1(\tau),\ldots,y_i(\tau),\ldots y_8(\tau))^{\rm T}, \tag{18}$$

where

$$\begin{aligned} y_i(\tau) \;=\; & \lim_{t\to\infty}[\langle\sigma^{\rm i}(t),\sigma_{32}(t+\tau)\rangle \\ & -\langle\sigma^{\rm i}(t)\rangle\langle\sigma_{32}(t+\tau)\rangle], \quad (i=1,2,\ldots,8). \end{aligned} \tag{19}$$

As we know, y_i and x_i satisfy the same set of equations. Using the Laplace transform method, we obtain a set of equations for $y_i^l(z)$, which is analogous to Eqs. (13). The initial values of $y_i^l(z)$ are given by

$$\begin{pmatrix} y_1^l(0)\\ y_2^l(0)\\ y_3^l(0)\\ y_4^l(0)\\ y_5^l(0)\\ y_6^l(0)\\ y_7^l(0)\\ y_8^l(0) \end{pmatrix} = \begin{pmatrix} 0\\ 0\\ 0\\ 0\\ \sigma_{21}(\infty)\\ 0\\ \sigma_{22}(\infty)\\ 0 \end{pmatrix} - \sum_{m=-\infty}^{\infty} \begin{pmatrix} \sigma_{11}^m(\infty)\sigma_{23}^{l-m}(\infty)\\ \sigma_{22}^m(\infty)\sigma_{23}^{l-m}(\infty)\\ \sigma_{21}^m(\infty)\sigma_{23}^{l-m}(\infty)\\ \sigma_{12}^m(\infty)\sigma_{23}^{l-m}(\infty)\\ \sigma_{31}^m(\infty)\sigma_{23}^{l-m}(\infty)\\ \sigma_{13}^m(\infty)\sigma_{23}^{l-m}(\infty)\\ \sigma_{32}^m(\infty)\sigma_{23}^{l-m}(\infty)\\ \sigma_{23}^m(\infty)\sigma_{23}^{l-m}(\infty) \end{pmatrix}. \tag{20}$$

The incoherent fluorescence spectrum can be calculated through

$$S_{\rm in}(\Delta_{\rm f}) = {\rm Re}[y_7^0(z)|_{z={\rm i}\Delta_{\rm p}}]. \tag{21}$$

In the following, we will present our numerical results. First we investigate the influences of the second biochromatic field on the absorption spectrum. We assume $\phi_{\rm A} = \phi_{\rm B} = 0$. For $\Omega_1 = \Omega_2 = \Omega_3 = \Omega_4 = 2.5$, a series of absorption spectra versus $\Delta_{\rm p}$ with different δ are plotted in Fig. 2. For $\delta = 7$, it is seen that the spectrum shows a multi-peaked profile, including a central peak and a set of sidebands located symmetrically, adjacent peaks are separated by an constant distance δ. Unlike the absorption spectrum of a two-level biochromatic-field-driven atom or a V-type atom driven by biochromatic fields,[20] the negative absorption components emerge for the inner sidebands, which give a sign of gain effects.

When δ increases, the amplitude of the central peak increase and the amplitudes of the sidebands degrade simultaneously. For an adequately large δ value ($\delta \gg 18$), the amplitudes of the sidebands are nearly zero, while the amplitude of the central peak reaches a comparatively high value, which shows a very strong absorption.

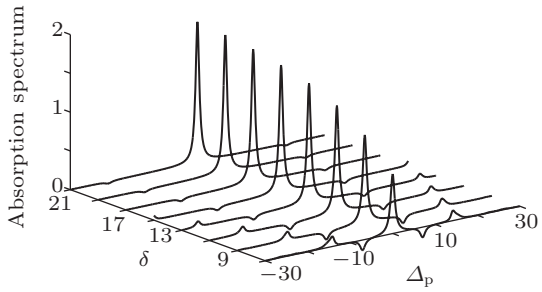


Fig. 2. Absorption spectrum corresponding to the 2–3 transition. The parameters are $\phi_{\rm A} = 0$, $\phi_{\rm B} = 0$, and $\Omega_1 = \Omega_2 = \Omega_3 = \Omega_4 = 2.5$.

In Fig. 3 we present the numerical results of the incoherent fluorescence spectrum when the second biochromatic field is on. We assume $\Omega_1 = \Omega_3 = \Omega$ and Ω is adjustable, and other parameters are the same as those in Fig. 2. When the intensity of second biochromatic field increases, the amplitude of the central peak deceases, the amplitude of inner sidepeaks increases, and the outer peaks remain nearly unchanged. When Ω keeps rising, this trend is continued, while at $\Omega = 6.5$ the amplitude of the inner sidebands is higher than that of the central peak. It can be deduced that the rising of the two inner peaks will lead to an enhancement of the total incoherent fluorescence spectrum intensity. With a further increase of Ω, the height of the inner sidepeaks begin to drop, which can be seen from the two curves on the top left side of Fig. 3. Correspondingly, this will lead to a reduction of the intensity of the incoherent fluorescence spectrum. The conclusion reached above is verified through Fig. 4. The intensity of the fluorescence of spontaneous transition increases for a moderately large driven field, at $\Omega = 7.8$, the intensity reach its maximum value and begin to drop down as long as Ω exceed the critical value.

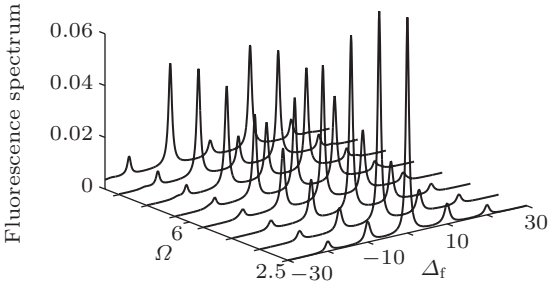


Fig. 3. Incoherent fluorescence spectrum corresponding to the 2–3 transition. The parameters are $|\Omega_2| = |\Omega_4| = 2.5$, $\phi_{\rm A} = 0$, $\phi_{\rm B} = 0$, and $|\Omega_1| = |\Omega_3| = \Omega$.

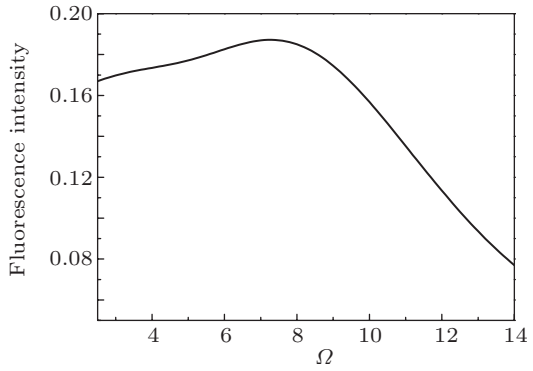


Fig. 4. Intensity of the incoherent fluorescence spectrum corresponding to the 2–3 transition. The parameters are $\phi_A = 0$, $\phi_B = 0, \Omega_1 = \Omega_3 = \Omega$, and $\Omega_2 = \Omega_4 = 2.5$.

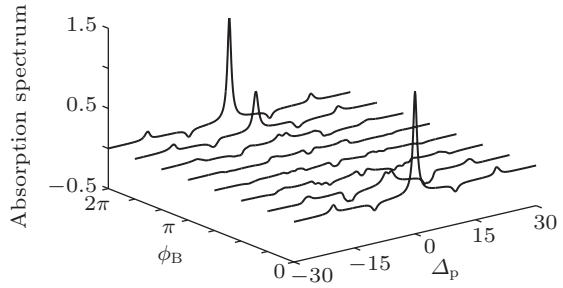


Fig. 5. Absorption spectrum corresponding to the 2–3 transition. The parameters are $\phi_A = 0$, and $|\Omega_1| = |\Omega_2| = |\Omega_3| = |\Omega_4| = 2.5$.

Next we present the numerical results of the absorption spectrum and incoherent fluorescence spectrum when phase modulating is implemented. In the numerical estimations we find that the spectra depend only on the sum of ϕ_A and ϕ_B, i.e., if the sum of the two phases is fixed, the spectrum is irrelevant to the individual value of ϕ_A or ϕ_B. For clarity, we designate ϕ as the sum of ϕ_A and ϕ_B. The series of absorption curves as the function of detuning Δ_p for several different values of ϕ are presented in Fig. 5. Observing the second curve from the right in which $\phi = 0.3\pi$, one can find that when ϕ surpass zero, a dip occurs on the top of the central peak. Simultaneously, inner gain peaks exhibit a two-peak feature. Also it can be seen that, in the range from 0 to π, the dip in the central peak is deepened while ϕ increases. Interestingly, when we keep increasing ϕ, the inner peaks are transmitted to triplets, which can be seen from the third line from the right side of Fig. 5. However, by inspecting the whole series of spectra, we find the most striking feature is the rapid decrease of the amplitude of the absorption spectrum. For $\phi = 0$, the amplitude of the central peak, inner sidepeaks, and outer sidepeaks are 1.3, -0.1, and 0.1, respectively. When $\phi = 0.4\pi$ (see the second curve from the right), the absorption amplitude for $\Delta_p = 0$ is 0.12 due to the splitting of the central peak. The location of the highest value of absorption amplitude deviate slightly from $\Delta_p = 0$, the value is 0.14. Further increasing the value of ϕ, we find that the spectrum begin to degrade overall. For $\phi = 0.8\pi$, the highest value of the overall spectrum is 0.025, which is about two orders of magnitude less than the maximal value for $\phi = 0$. As shown in Fig. 5, the attenuation ends at $\phi = \pi$, when the value of ϕ is over π, the amplitudes of the absorption increase along with the increase of ϕ.

In Fig. 6 we plot the fluorescence spectrum for several different values of ϕ, with other parameters remaining the same as in Fig. 5. As ϕ increases, it is seen that the splitting effect occurs to the spectral line. From the third line from the right ($\phi = 0.5\pi$), we can see the following facts: (i) a dip appears on the top of the central peak; (ii) the original inner sidebands are transformed into triplets, where two sidepeaks are located closely at the two sides of the central peak, and the two sidepeaks are asymmetric; (iii) similar to the central peak, the outer sidebands also experience splitting, the dip is located at $\Delta_f = \pm 2\delta$. As the value of ϕ increases, the depth of the dip on the central peak is enhanced, while the inner peaks of the triplets apparently degrade, and the triplets are transmitted to doublets. With a further increase of ϕ, it can be seen that the dips in the central line and outer sideband are filled up, and the peak values of the inner doublets reduce and the doublets merge into a single peak.

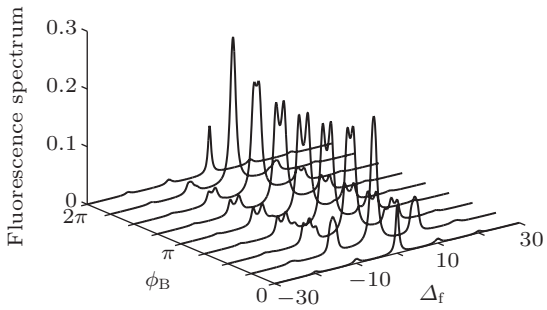


Fig. 6. Incoherent fluorescence spectrum corresponding to the 2–3 transition. The parameters are $\phi_A = 0$, and $|\Omega_1| = |\Omega_3| = |\Omega_2| = |\Omega_4| = 2.5$.

3. Dressed-state explanations

In order to give the dress-state explanations, the quantized Hamiltonian is considered here, which has the form

$$H = H_0 + V, \tag{22}$$

where

$$H_0 = \hbar(\omega_{12} + \omega_{23})\sigma_{11} + \hbar\omega_{23}\sigma_{22} + \hbar \sum_{i=1,2,3,4} \omega_i a_i^+ a_i \tag{23}$$

is the noninteracting atom-plus-field Hamiltonian. Therein, a_i is the annihilation operator of the laser mode i. Additionally, V is the interaction part in the form

$$\begin{aligned} V = & -\hbar g(a_1 \mathrm{e}^{-\mathrm{i}\omega_1 t + \mathrm{i}\phi_1} + a_3 \mathrm{e}^{-\mathrm{i}\omega_3 t + \mathrm{i}\phi_3})\sigma_{12} \\ & -\hbar g(a_2 \mathrm{e}^{-\mathrm{i}\omega_2 t + \mathrm{i}\phi_2} + a_4 \mathrm{e}^{-\mathrm{i}\omega_4 t + \mathrm{i}\phi_4})\sigma_{23} + \mathrm{c.c.} \end{aligned} \tag{24}$$

In the case of large δ, it has been demonstrated in the same model[10] that the eigenstates of the coupling system form two

two-photon absorption channels. There are four states in the dressed-state picture: the mutual top and bottom states are $|1\rangle$ and $|3\rangle$, and the intermediate states are denoted by $|+\rangle$ and $|-\rangle$ which are equal to $|2\rangle$ and $-|2\rangle$ in the case of large δ. Therefore, in our analysis, it is reasonable to only consider the Hamiltonian of the lower two states and the coupling between them. The corresponding part of Hamiltonian in the rotating frame mentioned in Section 2 is written as

$$H' = H'_0 + V', \tag{25}$$

where

$$\begin{aligned} H'_0 &= \hbar\omega_{23}\sigma_{22} + \hbar\sum_{i=2,4}\omega_i a_i^+ a_i, \\ V' &= -\hbar g(a_2\,\mathrm{e}^{\mathrm{i}\delta t} + a_4\,\mathrm{e}^{-\mathrm{i}\delta t - \mathrm{i}\phi_\mathrm{B}})\sigma_{23} + \mathrm{c.c.} \end{aligned} \tag{26}$$

According to the sequence we laid out the numerical results, we begin our discussion firstly by setting $\phi_\mathrm{B} = 0$. The bare states of the non-interacting Hamiltonian H'_0 are given by

$$|2, n_2 + n - 1, n_4 - n\rangle,\ \ |3, n_2 + n, n_4 - n\rangle,\ \ (n = 0, \pm 1, \ldots), \tag{27}$$

where n_2 and n_4 are the photon occupation numbers of field modes $\omega_{23} \pm \delta$. With different values of n, the energies of the upper bare states are different but simple calculations show that their energy values are all approximately $\hbar(n_2 + n_4)\omega_{23}$ under the condition $\delta \ll \omega$. Experimentally, this condition can be easily fulfilled. According to the method illustrated in Refs. [1] and [4], the eigenvalues of H' are given by

$$\lambda = m\delta, \quad (m = 0, \pm 1, \ldots), \tag{28}$$

the corresponding eigenvectors are

$$\boldsymbol{X}^m = (\ldots, X_n^m, \ldots, X_1^m, X_0^m, \ldots, X_{-n}^m, \ldots), \tag{29}$$

where

$$X_n^m = \mathrm{J}_{n-m}(-2\Omega/\delta), \tag{30}$$

and $\mathrm{J}_n(x)$ is the Bessel function of order n. Here we label the collection of these eigenstates of which the energies are close to $(n_2 + n_4)\hbar\omega$ as manifold $n_2 + n_4$.

The atom and the probe beam are coupled by the interaction $w = \boldsymbol{\mu}_{23} \cdot \boldsymbol{E}_\mathrm{p}$, where $\boldsymbol{E}_\mathrm{p}$ is the amplitude of the probe field. The permitted transitions induced by the probe beam between two manifolds occur between the states which have non-zero matrix elements of w. Meanwhile, the permitted spontaneous transitions occur between the dressed states of the two manifolds which has a nonzero μ_{23}. In manifold $n_2 + n_4$ and $n_2 + n_4 + 1$ these transitions occur between the eigenstates which are contaminated by $|2, n_2, n_4\rangle$, and $|3, n_2, n_4\rangle$, respectively.

In Figs. 2 and 3, the absorption spectrum and the fluorescence spectrum both have five components. However, from the above description of the dressed-atom model, there should be more components. This phenomenon can be explained as follows: for the small value of Ω/δ (≤ 0.25), $\mathrm{J}_n(-\Omega/\delta)$ ($n = 0, \pm 1, \ldots$) decreases by one order of magnitude when n increases or decreases by one from zero. Hence, it is reasonable to take an approximate form of the eigenstates which is given by

$$X^m = (\ldots, 0, \ldots, 0, X_{m+1}^m, X_m^m, X_{m-1}^m, 0, \ldots, 0, \ldots). \tag{31}$$

In manifold $n_2 + n_4 + 1$, the eigenstates are given by

$$\begin{aligned} X^1 &= \mathrm{J}_1|2, n_2 - 1, n_4 + 1\rangle + \mathrm{J}_0|3, n_2, n_4 + 1\rangle \\ &\quad + \mathrm{J}_{-1}|2, n_2, n_4\rangle, \\ X^0 &= \mathrm{J}_1|3, n_2, n_4 + 1\rangle + \mathrm{J}_0|2, n_2, n_4\rangle \\ &\quad + \mathrm{J}_{-1}|3, n_2 + 1, n_4\rangle, \\ X^{-1} &= \mathrm{J}_1|2, n_2, n_4\rangle + \mathrm{J}_0|3, n_2 + 1, n_4\rangle \\ &\quad + \mathrm{J}_{-1}|2, n_2 + 1, n_4 - 1\rangle, \end{aligned} \tag{32}$$

and in manifold $n_2 + n_4$

$$\begin{aligned} X^1 &= \mathrm{J}_1|3, n_2 - 1, n_4 + 1\rangle + \mathrm{J}_0|2, n_2 - 1, n_4\rangle \\ &\quad + \mathrm{J}_{-1}|3, n_2, n_4\rangle, \\ X^0 &= \mathrm{J}_1|2, n_2 - 1, n_4\rangle + \mathrm{J}_0|3, n_2, n_4\rangle \\ &\quad + \mathrm{J}_{-1}|2, n_2, n_4 - 1\rangle, \\ X^{-1} &= \mathrm{J}_1|3, n_2, n_4\rangle + \mathrm{J}_0|2, n_2, n_4 - 1\rangle \\ &\quad + \mathrm{J}_{-1}|3, n_2 + 1, n_4 - 1\rangle. \end{aligned} \tag{33}$$

Here $\mathrm{J}_m(-2\Omega/\delta)$ is shortened to J_m. Figure 7 shows the simplified sketch of the dressed states of two adjacent manifolds. It can be seen that all the transitions between the states in adjacent manifolds will make contributions to five components of which the frequencies are ω_{23}, $\omega_{23} \pm \delta$, and $\omega_{23} \pm 2\delta$, respectively.

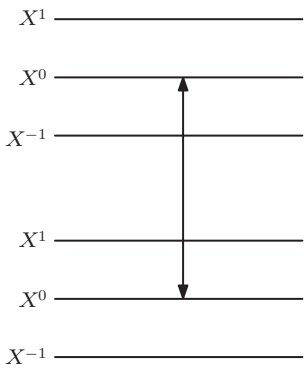


Fig. 7. Eigenstates of the dressed atom.

In the following we will use the model of the dressed states established above to interpret most of the results obtained numerically. The alteration in the fluorescence spectra for different values of Ω_1 and Ω_3 can be interpreted as: when

the strengths of Ω_1 and Ω_3 are adjusted to a value which are unequal to the values of Ω_2 and Ω_4, the condition under which the suppression of two-photon absorption is broken.[10] Hence the population probabilities of states $|1\rangle$ and $|2\rangle$ are increased, which results in an enhancement of the spontaneous transitions $|1\rangle \rightarrow |2\rangle$ and $|2\rangle \rightarrow |3\rangle$. For a very strong Ω_1 and Ω_3 ($\Omega_1, \Omega_3 > 8$), the coupling between $|1\rangle$ and $|2\rangle$ is stronger than that between $|2\rangle$ and $|3\rangle$. Therefore, the lower coupling can be ignored, and the eigenstates of the upper coupling Hamiltonian defines the dressed states of the whole system. In Fig. 8, we shows the scheme of the five channels of spontaneous transitions. The eigenstates are easily obtained by using the above mentioned method so they are not given here. Through some straight calculations, we found that the population probabilities of Y^2, Y^0, and Y^{-2} are equal, and the population probabilities of Y^1 and Y^{-1} are equal. For the parameter values $\Omega_1 = \Omega_3 = 8$ and $\Omega_2 = \Omega_4 = 2.5$, $P_{Y^2} = 0.05$, and $P_{Y^1} = 0.07$. Correspondingly, in Fig. 3, for $\Omega = 9.5$, the central peak and outer peaks have the same amplitudes and are lower than the inner sidepeaks. When Ω_1 and Ω_3 keep increasing, the population in $|1\rangle$ keeps increasing, which will lead to a reduction of the population in $|2\rangle$ and $|3\rangle$, and further result in the reduction of the intensity of the fluorescence spectrum shown in Fig. 4.

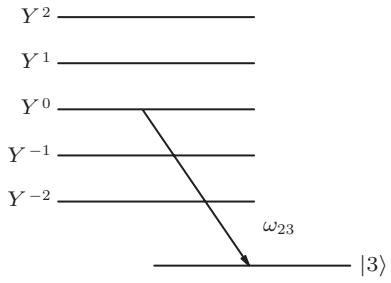


Fig. 8. Scheme of the channels of spontaneous transitions.

The phenomenon of transformation from a multipeaked profile to a single-peak profile shown in Fig. 2 can be interpreted as: for a large δ, $J_1 \approx 0$, $J_{-1} \approx 0$, and $J_0 \approx 1$. In manifolds $n_2 + n_4$ and $n_2 + n_4 + 1$ $X^0 \approx |3, n_2, n_4\rangle$ and $X^0 \approx |2, n_2, n_4\rangle$, respectively. The transition between these two states is the only transition in which the probe induces so that there is only one absorption peak at $\Delta_p = 0$. When a nonzero value of ϕ_B is considered, it is difficult to obtain the analytical solutions. We will present an explanation by exploring the numerical formulation (13). On the basis of Eqs. (13), employing the parameter values used in Fig. 3, we can write the absorption spectrum of $|3\rangle \rightarrow |2\rangle$ as

$$A(\Delta_p) = 2(\rho_{33}^0 - \rho_{22}^0) + \mathrm{Re}[U^0(z)|_{z=-i\Delta_p}], \qquad (34)$$

where U^0 represents the collection of the terms excluding $x_7^0(z)$. In our calculations (not given here) the value of the first term dominates the expression (34). From Eq. (34), we can state that the amplitude of the absorption spectrum is directly relevant to the zero-order component of the population difference $\rho_{33}^0 - \rho_{22}^0$. In Fig. 9, we illustrate the population ρ_{22} and ρ_{33} as the function of ϕ_B. It is seen that from $\phi_B = 0$ the values of population ρ_{33} begin decreasing while ρ_{22} begin increasing. At approximately $\phi_B = 0.7\pi$, both two populations reach their comparatively stable values. Additionally, at a range of ϕ_B form 0.7π to 1.1π, the difference between the two values is very small. This exactly reflects the changes in spectra shown in Fig. 5, where an obvious suppression of the absorption spectrum at the same range of ϕ_B is presented. Beyond 1.1π, the difference begins to increase, which leads to the recovering of the absorption spectrum.

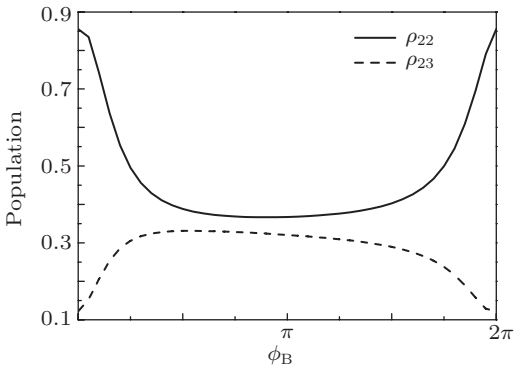


Fig. 9. Population versus ϕ_B for ρ_{22} and ρ_{33}.

4. Summary

To sum up, in this paper, we investigated the absorption spectrum and the incoherent fluorescence spectrum of the lower transition of a Ξ-configuration system driven by two bichromatic fields. We studied the influences of the intensity of the second bichromatic field and the phase difference between the applied fields on the spectral properties of the system. We see that both the absorption spectrum and the fluorescence show a multi-peaked structure, and adjacent peaks have a constant separation. For the fluorescence spectrum, when the intensity of the second bichromatic increases, the heights of the central peaks and outer sidepeaks decrease while that of the inner peaks increase. Meanwhile, the whole intensity of the incoherent fluorescence spectrum increases. In a dress-state analysis, it is proved that these are due to the transformation of the dressed-states structures created by different parts of the Hamiltonian. For the absorption spectrum, when the value of detuning increases, we found the multipeaked absorption spectrum are changed into a single high peak. In a dressed-state analysis it is shown that this is due to the transition between different states when δ increases. When phase is taken into account, in the fluorescence spectrum a dip emerges in the central peak, while the inner sidebands are transmitted to

triplets. To the absorption spectrum, we found that the absorption spectrum will experience a strong attenuation when the relative phase of the driven bichromatic field changes. Numerically, the average amplitudes of spectrum is about 70 times less than the amplitude of the single peak in the case of large δ, therefore we can reach the conclusion that the medium is nearly transparent to the probe field. The two fields applied to the same transition can be set counter-propagating in a real experiment, and this will effectively eliminate the Doppler-broadening in the atomic vapor.

References

[1] Freedhoff H and Chen Z 1990 *Phys. Rev.* A **41** 6013
[2] Zhu Y, Lezama A, Wu Q and Mossberg T W 1989 *Coherent and Quantum Optics VI* (New York: Plenum) p. 1297
[3] Tewari S P and Kumari M K 1990 *Phys. Rev.* A **41** 5273
[4] Agarwal G S, Zhu Y, Gauthier D J and Mossberg T E 1991 *J. Opt. Soc. Am.* B **8** 1163
[5] Ficek Z, Seke J, Soldatov A V and Adam G 2001 *Phys. Rev.* A **64** 013813
[6] Kryuchkyan G Yu, Jakob M and Sargsian A S 1998 *Phys. Rev.* A **57** 2091
[7] Yoon T H, Chung M S and Lee H W 1999 *Phys. Rev.* A **60** 2547
[8] Wang J, Zhu Y, Jiang K J and Zhan M S 2003 *Phys. Rev.* A **68** 063810
[9] Yang L J, Zhao M, Zhang L S, Feng X M, Li X L and Wei C J 2010 *Chin. Phys.* B **19** 084204
[10] Zou J H, Hu X M, Cheng G L, Li X and Du D 2005 *Phys. Rev.* A **72** 055802
[11] Hu X M, Cheng G L, Zou J H, Li X and Du D 2005 *Phys. Rev.* A **72** 023803
[12] Hu X M, Shi W X, Xu Q, Guo H J, Li J Y and Li X X 2006 *Phys. Lett.* A **352** 543
[13] Li Z H, Li Y, Dou Y F and Zhang J X 2012 *Chin. Phys.* B **21** 034204
[14] Li J Y and Hu X M 2009 *Phys. Rev.* A **80** 053829
[15] Wu H, Wang Y L and Ding L E 2010 *Acta Phys. Sin.* **59** 3978 (in Chinese)
[16] Cox K, Yudin V I, Taichenachev A V, Novikova I and Mikhailov E E 2011 *Phys. Rev.* A **83** 015801
[17] Honda K, Kobayashi Y and Morinaga A 2007 *Phys. Rev.* A **75** 023607
[18] Lu Y Y, Zeng Z N, Zheng Y H, Zou P, Liu C D, Gong C, Li R X and Xu Z Z 2011 *Acta Phys. Sin.* **60** 103202 (in Chinese)
[19] Zhang J P, Xu J, Hernandez G, Hu X M and Zhu Y F 2007 *Phys. Rev.* A **75** 043810
[20] Li P, Nakajima T and Ning X J 2006 *Phys. Rev.* A **74** 043408
[21] Wanare H 2006 *Phys. Rev. Lett.* **96** 183601
[22] Guo H J, Niu Y P, Wang L C, Jin S Q and Gong S Q 2008 *Chin. Phys. Lett.* **25** 3656
[23] Zhou B and Li S M 2010 *Chin. Phys.* B **19** 033401
[24] Brabec T and Krausz F 2000 *Rev. Mod. Phys.* **72** 545
[25] Sansone G, Vozzi C, Stagira S, Pascolini M, Poletto L, Villoresi P, Tondello G, de Silvestri S and Nisoli M 2004 *Phys. Rev. Lett.* **92** 113904
[26] Nakajima T and Watanabe S 2006 *Phys. Rev. Lett.* **96** 213001